RSC Advances

ROYAL SOCIETY OF CHEMISTRY

www.rsc.org/advances

Adsorption of Aromatics on the (111) Surface of PtM and PtM_3 (M = Fe, Ni) Alloys

Alyssa J. R. Hensley[a], *Sebastian Schneider*[a], *Yong Wang*[a,b], *and Jean-Sabin McEwen*[a,c,d]*

[a] The Gene & Linda Voiland School of Chemical Engineering and Bioengineering, Washington State University, Pullman WA 99164

[b] Institute for Integrated Catalysis, Pacific Northwest National Laboratory, Richland, WA, 99352

[c] Department of Physics and Astronomy, Washington State University, Pullman, WA 99164

[d] Department of Chemistry, Washington State University, Pullman, WA 99164

**Corresponding author:* Jean-Sabin McEwen; 509-335-8580 (phone), 509-335-4806 (fax), js.mcewen@wsu.edu

Abstract

The adsorption of benzene and phenol was studied on PtM and PtM_3 (111) surfaces, with M being either Ni or Fe. Under vacuum, the most favorable near surface structures showed an enrichment in Pt over the M species. An analysis of the electronic structure of the metal species in the clean surfaces with different near surface structures was done with the d-band model and showed that the Pt's d-states are significantly shifted away from the Fermi level due to the Pt-M interactions while the M species' d-states were less affected, with Ni's d-band shifting closer to the Fermi level and Fe's d-band shifting away from the Fermi level. The adsorption of aromatics, benzene and phenol, on several near surface structures for the PtM and PtM_3 (111) surfaces showed that higher surface M concentrations resulted in a stronger adsorption due to the larger amount of charge transferred between the adsorbate and surface. However, compared to the adsorption of benzene and phenol on monometallic surfaces, the adsorption of these species on the PtM and PtM_3 (111) surfaces was significantly weakened. Overall, our results show that the

observed behavior of these Pt/Fe and Pt/Ni alloys is similar to that seen for the previously studied Pd/Fe surfaces. Furthermore, balancing the weakly adsorbing Pt surface species with the more strongly interacting Fe or Ni species can lead to the tailored adsorption of aromatics with applications in both hydrodeoxygenation and hydrogenation reactions by increasing the desorption rate of wanted aromatic products.

Keywords

PtM (111) Alloys, PtM_3 (111) Alloys, Base Metal Surfaces, Surface Segregation Trends, Aromatic Adsorption, Base Metal-Noble Metal Bimetallic Surfaces, Benzene Adsorption, Phenol Adsorption

1. Introduction

Pt is a highly useful metal with applications in catalytic converters[1], fuel cells[2], and biomass upgrading[3] due to its high catalytic activity for oxidation and hydrogenation reactions[4]. Specifically in the application of Pt to the conversion of bio-oil to useable biofuels, Pt's activity for both dissociating H_2 to surface H species and hydrogenating unsaturated hydrocarbons is useful for the removal of oxygen from the bio-oils, which causes the bio-oils to have lower energy densities, lower thermal stabilities, and higher viscosities.[5] However, Pt alone does not remove the majority of the oxygen from the bio-oil.[6, 7] Recent work has shown that the addition of a small amount of noble metal, such as Pd or Pt, to a bulk Fe catalyst can significantly improve the activity and deoxygenation selectivity of the bimetallic catalyst.[7, 8] The combination of the noble metal dopant and Fe catalyst has been shown to maintain the activity of the Fe surface,[8] which easily deactivates by forming oxides and carbides when acting alone as a catalyst[9]. In our previous work on Pd/Fe surfaces,[7, 10] we observed that the Pd dopant's electronic structure was significantly affected by the Pd-Fe interactions, leading it to be deactivated for

aromatic adsorption. Furthermore, the weakened adsorption of aromatics on the surface Pd suggest that the active site for the HDO of phenolics is likely to be exposed Fe. Here, we expand upon our previous work by studying low concentration Pt alloys containing either Fe or Ni as both types of bimetallic catalysts have been shown to have a high activity and hydrodeoxygenation (HDO) selectivity for m-cresol.[8, 11] As the noble metals are known to surface segregate in the Fe host[10, 12, 13], the creation of bimetallic catalysts with Pt as a dopant can significantly decrease the cost of the catalyst without sacrificing catalytic performance.

Numerous studies have examined improving the performance, stability, or selectivity of Pt surfaces by introducing a small amount of an impurity in the form of creating Pt_3M alloys. Under vacuum conditions, Pt_3M surfaces have shown to preferentially segregate Pt to the surface layers with the majority of transition metal dopants.[14-19] However, the Pt's electronic character is changed by the presence of the second metal[20] which could lead to a change in surface to adsorbate interactions that can be predicted using the d-band model[21, 22]. The presence of adsorbates on the Pt_3M alloy surface has the potential to rearrange the surface structure if strong adsorbate-M interactions are present. For adsorbates such as S, CO, benzene, or H, these strong adsorbate-M interactions do not occur and the observed Pt surface segregation behavior of the Pt_3M alloys is consistent with that seen in vacuum.[16, 23, 24] Other adsorbates, such as Cl and N, have the potential to reverse the surface segregation behavior of Pt in Pt_3M alloys with a small number of M dopants, such as Ru and Ir for N and Fe and Ni for Cl.[23, 25] Finally, adsorbates such as O and OH have strong adsorbate-M interactions which result in a reversal of the Pt surface segregation trend for almost all M dopants in the Pt_3M alloys.[17, 23, 26] Overall, these results show that much is known about the Pt_3M alloy system and the surface composition under many different conditions.

As the above discussion shows, a significant amount of the work on Pt alloys has been performed on the Pt_3M alloys as these are of significant interest to electrochemical applications. However, alloys of lower Pt concentration are gaining interest in other areas, like bio-oil upgrading, in order to reduce the cost of catalysts while maintaining the high catalytic activity of Pt. Previous experimental work on these lower Pt concentration alloys (PtM and PtM_3) has shown that the trend of Pt surface segregation under vacuum observed in the Pt_3M alloys continues in the PtM and PtM_3 alloys.[14, 19, 27] Furthermore, surfaces with Pt surface segregation have been shown to be more resistant to acidic environments, supporting the use of such Pt surface alloys in electrochemical applications.[28, 29] Theoretical work has shown that the segregation behavior of lower Pt concentration alloys can depend on the exposed surface facet[30] and that the subsurface concentration of the M species can alter the catalytic activity of the Pt surface layer for the oxygen reduction reaction[20]. While these results provide insight into the surface structure of lower Pt concentration alloys under vacuum and the effect that these structure variations can have on a single type of reaction, much is still unknown about the effect of various adsorbates on the Pt alloy near surface structure and the effect of the near surface structure on various adsorbates and their reactions.

In this work, we study the adsorption of benzene and phenol on PtM and PtM_3 (111) surfaces with different degrees of the surface segregation of the Pt and M species, where M is either Ni or Fe. Five distinct near surface structures were examined under vacuum for both the PtM and PtM_3 (111) surface and the segregation behavior and its effect on the Pt and M species electronic structure was characterized. The several most favorable near surface structures from the vacuum studies were then studied with the adsorption of both benzene and phenol in order to determine both the surface and subsurface composition effect on aromatic adsorption.

Furthermore, the surface to adsorbate electronic interactions were characterized in order to gain a deeper understanding of the adsorbate's effect on the surface segregation behavior in the PtM and PtM_3 (111) surfaces. Overall, these results show that Pt has a strong tendency to surface segregate in PtM and PtM_3 (111) alloys, similar to the Pt_3M alloy, but decreasing the overall Pt concentration in the alloy results in the formation of mixed Pt and M surface layers. The electronic analyses show that the adsorption of aromatics is stronger on the more M rich surfaces. However, compared to the adsorption of benzene and phenol on monometallic surfaces, the PtM and PtM_3 (111) surfaces adsorb aromatics to a weaker degree. This behavior of weakening the adsorption energy of aromatics on Pt/Fe and Pt/Ni surfaces is and likely contributes to the improved HDO capability of the bimetallic surfaces by the desorption rate of the wanted aromatic products, which could otherwise decompose into carbon fragments that poison the surface. Finally, this work shows that the trends in the surface electronic structures and adsorption of aromatics found for Pd/Fe surfaces[7, 10] is extendable to other noble metal doped, base metal surfaces, such as Pt/Fe and Pt/Ni surfaces.

2. Methods

All calculations were performed using the Vienna Ab Initio Simulation Package[31, 32] and the computational details used here are identical to those previously used by the authors[10]. The effect of van der Waals corrections are examined by comparing results obtained with the generalized gradient approximation (GGA) in the form of the Perdew, Burke, and Ernzerhof (PBE)[33, 34] functional with those obtained using the optB88-vdW[35, 36] functional. All calculations were performed with the Methfessel-Paxton[37] (N=1) smearing method with a smearing width of 0.1 eV to improve convergence, and the total energy was extrapolated to zero Kelvin. As Fe and Ni are known to be ferromagnetic and O is a spin polarized atom, spin polarization effects were accounted for in all calculations. In addition to these factors, the effect of dipole interactions

between the consecutive supercells was considered to be significant and dipole corrections were imposed in each calculation performed.[38]

2.1 Bulk Structure

The bulk alloy structures were optimized using a Monkhorst-Pack[39] (10x10x10) grid. The two alloys studied here are the PtM and PtM_3 alloys, where M is either Fe or Ni. Previous work has shown that the PtM alloys have the $L1_0$ structure, with two lattice constants (a_0 and c), while the PtM_3 alloys have the $L1_2$ structure, with one lattice constant (a_0).[19, 40, 41] These structures were used to calculate the optimum lattice parameters, which are given in Table 1. The calculated bulk parameters for the alloys without van der Waals corrections are in good agreement with previous results, both theoretical and experimental,[40, 42] and the change in the exchange-correlation functional from the PBE to the optB88-vdW functional was found to not significantly alter the bulk parameters for these alloys, with the largest change in lattice constants found for the PtNi alloy, with a_0 increasing by 0.2%. For the following calculations, the appropriate lattice constants were used in order to match the functional being used (e.g. PBE versus optB88-vdW).

Table 1. Key parameters for the bulk PtM and PtM_3 (M = Fe, Ni) lattices calculated with the PBE (optB88-vdW) functional.[a]

System	a_0 (Å)	c/a_0	μ_M (μ_B)	μ_{Pt} (μ_B)
PtFe	3.859 (3.859)	0.976 (0.976)	2.93 (2.88)	0.35 (0.35)
$PtFe_3$	3.740 (3.738)	1.000 (1.000)	2.72 (2.69)	0.35 (0.36)
PtNi	3.849 (3.858)	0.945 (0.940)	0.76 (0.72)	0.36 (0.36)
$PtNi_3$	3.660 (3.660)	1.000 (1.000)	0.72 (0.69)	0.37 (0.37)

[a]primary lattice constant, a_0; ratio of secondary and primary lattice constants, c/a_0; magnetic moment of the metal M, μ_M; magnetic moment of Pt, μ_{Pt}.

2.2 Surface Segregation

The surface segregation models were constructed from the (111) facet of the PtM and PtM_3 alloys. The size of the supercells was chosen to be p(4x4) and six atomic layers were

employed to represent the near surface of the alloys. The bottom two layers were kept fixed into their bulk positions and all other atoms were allowed to fully relax and a vacuum spacing of ~14 Å was introduced in order to model the (111) surface. A Monkhorst-Pack[39] (3x3x1) k-point grid was used for the energetic analyses and this grid was increased to (5x5x1) for the calculation of the density of states. The surface segregation trends in the PtM and PtM_3 alloys were examined by altering the composition of the near surface layers by either moving subsurface Pt or M to the surface. Each model studied here was evaluated using the segregation energy as defined as:

$$E_{seg} = \frac{E_{slab,seg} - E_{slab}}{n} \quad (1)$$

where $E_{slab,seg}$, E_{slab}, and n are the total energy of the segregated slab model, the total energy of the original slab, and the number of atoms segregating to the surface. The change in the Pt and M component's d-states were quantified by calculating the specific metal's d-band center and width as defined by:

$$\varepsilon_d = \frac{\int_{-\infty}^{\varepsilon_{Fermi}} E\rho(E)dE}{\int_{-\infty}^{\varepsilon_{Fermi}} \rho(E)dE} \quad (2)$$

$$w_d = \left(\frac{\int_{-\infty}^{\varepsilon_{Fermi}} E^2\rho(E)dE}{\int_{-\infty}^{\varepsilon_{Fermi}} \rho(E)dE} \right)^{\frac{1}{2}} \quad (3)$$

where E is the given energy, ρ(E) is the density of electronic states at the given energy, and ε_{Fermi} is the Fermi level.

2.3 Aromatic Adsorption

Once the most energetically favorable near surface structures of the PtM and PtM_3 alloys were identified, benzene was adsorbed onto the model (111) surfaces. The surface adsorption models were chosen to be p(4x4) supercells and five atomic layers were employed to represent the near surface structure. The bottom three layers were kept fixed into their bulk positions and

all other atoms, including the adsorbate, were allowed to fully relax. A vacuum spacing of ~16 Å was introduced in order to minimize the interactions between periodic images and a Monkhorst-Pack[39] (3x3x1) k-point grid was used. We have tested the k-point grid using the B30°-NiNi site for benzene on the PtNi (111) surface (see section 3.2.1 for more details) using a (5x5x1) grid and we found that the adsorption energy only changed by 9 meV.

The energies of the various adsorption sites and structures were evaluated using the adsorption and distortion energies as defined as:

$$E_{ads} = E_{Total} - E_{Molecule} - E_{Surface} \quad (4)$$

$$E_{dist} = E_{Molecule}^{Distorted\ Geometry} - E_{Molecule}^{Free\ Gas\ Geometry} \quad (5)$$

where E_{Total}, $E_{Molecule}$, and $E_{Surface}$ are the total energies for the adsorption system, gas phase molecule, and surface, respectively, and $E_{Molecule}^{Distorted\ Geometry}$ and $E_{Molecule}^{Free\ Gas\ Geometry}$ are the total energies of the gas phase molecule with its surface distorted geometry and fully optimized geometry, respectively. The stronger the surface to adsorbate interactions, the greater the adsorbate will be distorted from its gas phase structure and the larger the value of E_{dist}. Previous work has shown that the presence of adsorbates can alter the segregation behavior of bimetallic surfaces.[24, 26, 43-45] Therefore, the surface segregation trend was investigated for the PtM and PtM_3 (111) alloy in the presence of benzene and phenol.

The electronic interaction between the surface and adsorbates will be evaluated using the differential charge density as defined as:

$$\Delta\rho = \rho_{adsorbate+surface} - \rho_{surface} - \rho_{adsorbate} \quad (6)$$

where $\rho_{adsorbate+surface}$, $\rho_{surface}$, and $\rho_{adsorbate}$ are the charge distributions for the optimized structure of the adsorbed system and the surface and gas phase adsorbate fixed in their adsorption

geometries. In addition to these qualitative analyses, the mean charge displacement upon adsorption was calculated using:[46, 47]

$$Q = \frac{1}{2}\int d\vec{r}\,|\Delta\rho(\vec{r})| \quad (7)$$

where $\Delta\rho(\vec{r})$ is the differential charge density of the system.

3. Results and Discussion

3.1 Near Surface Structure

As surfaces are being formed from bulk bimetallic alloys, there is likely to be a thermodynamic driving force for the preferential segregation of one metal over the other due to the relative surface energies and sizes of the atoms. This segregation driving force can potentially be altered by the presence of adsorbates and if the change in the segregation energy is large enough, the presence of the adsorbate could potentially alter the surface structure during catalysis. In the PtM and PtM_3 alloys, the near surface structure can either be enriched in the Pt or the M components or remain fixed into its non-segregated configuration. Several near surface structures were examined, in the absence and presence of benzene and phenol adsorbates, in order to determine the most favorable near surface structure of the PtM and PtM_3 alloys on the (111) surfaces, as shown in Figures 1 and 2. For all of the systems studied here, the effect of van der Waals corrections on the near surface structure of the surfaces was determined by comparing the segregation energies (Equation 1) calculated both with the PBE and optB88-vdW functionals.

First, we examined the PtM (111) alloy and the various near surface structures studied are shown in Figure 1. The possible segregation behavior of the PtM (111) surfaces were examined using five structures: a non-segregated PtM surface (Figure 1A), a partially Pt segregated $Pt_3M/PtM_3/PtM$ surface (Figure 1B), a completely Pt segregated Pt/M/PtM surface (Figure 1C), a 2 ML Pt segregated Pt/Pt/M/M/PtM surface (Figure 1D), and a partially M segregated

$PtM_3/Pt_3M/PtM$ surface (Figure 1E). The relative stability of each of these surfaces was evaluated using the segregation energy (Equation 1) and the results are shown in Table 2. Both the PtFe and PtNi surfaces show that the surface segregation of Pt is more favorable than the non-segregated near surface structure (Figure 1A). The most favorable near surface structure is the Pt/M/PtM surface (Figure 1C), where none of the M component is present in the surface. This result is consistent with experimental results for the PtNi (111) surface[14, 19] and previous theoretical work for a single Pt atom impurity in an Ni (111) or Fe (110) host[12]. However, this favorability is not significantly larger than the original PtM near surface structure or the partially Pt segregated $Pt_3M/PtM_3/PtM$ surface (Figure 1B). The large thermodynamic instability caused by either the formation of the double Pt surface layer (Figure 1D) or the surface segregation of the M component (Figure 1E) in the PtM alloys make the formation of these two surface structures highly unlikely. The addition of the van der Waals corrections does not significantly affect the segregation energy for the majority of the surfaces with only the $Pt_3Ni/PtNi_3/PtNi$ and Pt/Ni/PtNi surfaces slightly affected. The $Pt_3Ni/PtNi_3/PtNi$ surface becomes thermodynamically more favorable than the original PtNi surface while the thermodynamic stability of the Pt/Ni/PtNi surface decreases slightly with the inclusion of van der Waals effects. Due to the similar energies, under vacuum and aromatic adsorption, between the PtM, Pt/M/PtM, and $Pt_3M/PtM_3/PtM$ surfaces, further analyses were performed on each of these structures.

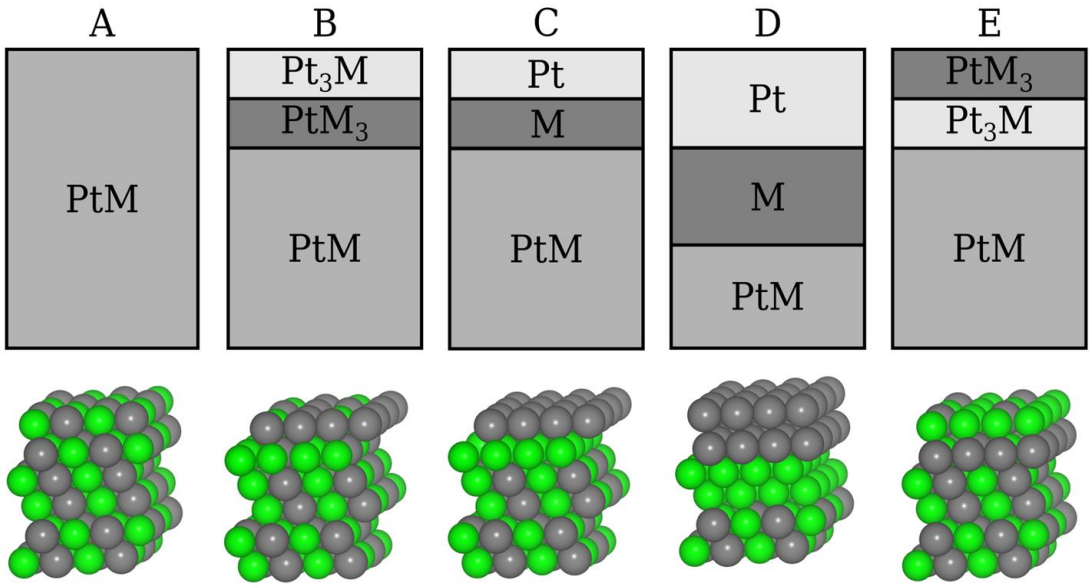

Figure 1. Studied near surface, segregation structures of the PtM alloys (M = Fe, Ni) for the PtM (111) surface. The surface structures are the non-segregated PtM surface (A), the slightly Pt enriched $Pt_3M/PtM_3/PtM$ surface (B), the 1 ML Pt enriched Pt/M/PtM surface (C), the 2 ML Pt enriched Pt/Pt/M/M/PtM surface (D), and the slightly M enriched $PtM_3/Pt_3M/PtM$ surface (E). The grey and green spheres represent the Pt and M components, respectively.

Table 2. Segregation energy for several possible near surface structures of the PtM and PtM_3 (M = Fe, Ni) (111) surfaces. The values calculated for the vacuum systems were performed using the PBE/optB88-vdW functionals while only the optB88-vdW functional was used for the adsorption systems. The energy values have units of eV/atom.

PtFe				**PtNi**			
Surface	Vacuum	Benzene	Phenol	Surface	Vacuum	Benzene	Phenol
PtFe	0.00/0.00	0.00	0.00	PtNi	0.00/0.00	0.00	0.00
$Pt_3Fe/PtFe_3/PtFe$	0.09/0.08	0.18	0.17	$Pt_3Ni/PtNi_3/PtNi$	0.08/-0.08	0.04	0.05
Pt/Fe/PtFe	-0.11/-0.09	-0.05	-0.06	Pt/Ni/PtNi	-0.21/-0.13	-0.06	-0.07
Pt/Pt/Fe/Fe/PtFe	0.73/0.71	-	-	Pt/Pt/Ni/Ni/PtNi	0.39/0.42	-	-
$PtFe_3/Pt_3Fe/PtFe$	1.10/1.10	-	-	$PtNi_3/Pt_3Ni/PtNi$	0.75/0.75	-	-
$PtFe_3$				**$PtNi_3$**			
Surface	Vacuum	Benzene	Phenol	Surface	Vacuum	Benzene	Phenol
$PtFe_3$	0.00/0.00	0.00	0.00	$PtNi_3$	0.00/0.00	0.00	0.00

$PtFe/Fe/PtFe_3$	-0.24/-0.21	-0.06	-0.08	$PtNi/Ni/PtNi_3$	-0.16/-0.11	0.06	0.06
$PtFe/PtFe/Fe/Fe/PtFe_3$	0.20/0.22	-	-	$PtNi/PtNi/Ni/Ni/PtNi_3$	0.31/0.34	-	-
$Pt/Fe/Fe/Fe/PtFe_3$	0.09/0.16	-	-	$Pt/Ni/Ni/Ni/PtNi_3$	0.30/0.37	-	-
$Fe/Pt/Fe/Fe/PtFe_3$	0.94/0.98	-	-	$Ni/Pt/Ni/Ni/PtNi_3$	0.85/0.89	-	-

Second, we examined the PtM_3 (111) alloy and the various near surface structures studied are shown in Figure 2. The possible segregation behavior of the PtM_3 (111) surfaces were examined using five structures: a non-segregated PtM_3 surface (Figure 2A), a partially Pt segregated $PtM/M/PtM_3$ surface (Figure 2B), a larger Pt segregated $PtM/PtM/M/M/PtM_3$ surface (Figure 2C), a completely Pt segregated $Pt/M/M/M/PtM_3$ surface (Figure 2D), and a completely M segregated $M/Pt/M/M/PtM_3$ surface (Figure 2E). The relative stability of these surfaces was evaluated using the segregation energy (Equation 1) and the results are shown in Table 2. Both the $PtFe_3$ and $PtNi_3$ surfaces show that the surface segregation of Pt is more favorable than the non-segregated near surface structure (Figure 2A). The most favorable near surface structure is the $PtM/M/PtM_3$ surface (Figure 2B), which is consistent with experimental results for the $PtNi_3$ (111) surface[14, 19] and previous theoretical work for a single atom impurity in host Ni (111) or Fe (110)[12]. Further surface segregation of Pt beyond a 50 % Pt surface is highly unfavorable due to the fact that further Pt surface segregation would require the Pt diffusing through three subsurface layers, significantly destabilizing the alloy. The effects of van der Waals corrections were also examined, but as can be seen by examining Table 2, they do not significantly alter the segregation energies for the PtM_3 alloys. Due to the similar energies between the PtM_3 and $PtM/M/PtM_3$ surfaces, further analyses were performed on each of these structures.

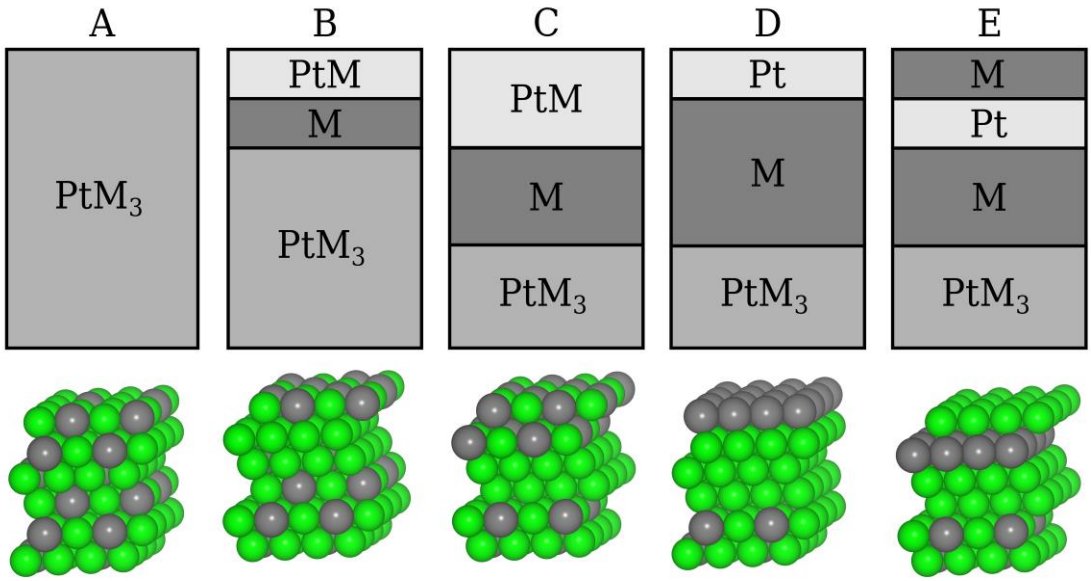

Figure 2. Studied near surface, segregation structures of the PtM_3 alloys (M = Fe, Ni) for the PtM_3 (111) surface. The surface structures are the non-segregated PtM_3 surface (A), the slightly Pt enriched $PtM/M/PtM_3$ surface (B), the Pt enriched $PtM/PtM/M/M/PtM_3$ surface (C), the 1 ML Pt enriched $Pt/M/M/M/PtM_3$ surface (D), and the 1 ML M enriched $M/Pt/M/M/PtM_3$ surface (E). The sphere coloring is identical to that shown in Figure 1.

The electronic structure of a metal surface's d-states have been shown to differ significantly in bimetallic surfaces compared to monometallic surfaces and these changes in the surface element's electronic structure can be used to understand and tailor the adsorption strength and characteristics of the surface to produce surfaces with optimum properties.[10, 21, 22] In order to better quantify the adsorption of aromatics on the most favorable near surface structures of the PtM and PtM_3 (111) alloys, the density of states for the Pt, Ni, and Fe in the alloys were calculated and their d-band properties were compared to those calculated for the monometallic Pt (111), Ni (111), and Fe (110) surfaces. The d-band properties calculated using Equations 2 and 3 and under vacuum for these surfaces are shown in Table 3, as well as the changes in the d-band

properties for the surface metal species in the alloys relative to the appropriate pure metal surfaces.

Table 3. The d-band center (ε_d, eV) and width (w_d, eV) for the Pt and M (Ni and Fe) species, as well as the change in both parameters ($\Delta\varepsilon_d$ and Δw_d, eV) relative to the appropriate pure metal surface (Pt, Ni, or Fe), in the three most favorable PtM (111) surfaces and two most favorable PtM_3 (111) surfaces.

Surface	Pt Species				M Species			
	ε_d	$\Delta\varepsilon_d$	w_d	Δw_d	ε_d	$\Delta\varepsilon_d$	w_d	Δw_d
PtFe	-2.81	-0.37	3.16	0.25	-2.32	-0.52	2.68	0.55
$Pt_3Fe/PtFe_3/PtFe$	-2.97	-0.53	3.34	0.43	-2.35	-0.55	2.72	0.59
Pt/Fe/PtFe	-3.20	-0.76	3.61	0.69	-	-	-	-
PtNi	-2.69	-0.25	3.10	0.18	-1.50	0.22	1.88	-0.14
$Pt_3Ni/PtNi_3/PtNi$	-2.88	-0.44	3.31	0.40	-1.56	0.24	1.96	-0.06
Pt/Ni/PtNi	-3.05	-0.61	3.55	0.63	-	-	-	-
$PtFe_3$ (111)	-2.99	-0.55	3.26	0.26	-2.02	-0.22	2.39	0.26
$PtFe/Fe/PtFe_3$	-3.17	-0.73	3.53	0.55	-2.14	-0.34	2.52	0.39
$PtNi_3$ (111)	-2.84	-0.40	3.18	0.35	-1.65	0.07	1.99	-0.03
$PtNi/Ni/PtNi_3$	-2.44	-0.60	3.47	0.61	-1.65	0.06	2.04	0.01

Pt (111), Ni (111), and Fe (110) surface species (used as references for $\Delta\varepsilon_d$ and Δw_d) have: d-band centers of -2.44 eV, -1.72, and -1.80 eV, respectively; and d-band widths of 2.92, 2.02, and 2.13, respectively.

Upon examining the Pt surface species trends, three things become apparent. First, the Pt-M interactions result in a shift of the Pt's d-band center to lower energies (away from the Fermi level) relative to Pt in the Pt (111) surface. The direction of the shift in the d-band center is consistent with previous work on both Pt[21] and Pd[10] bimetallic surfaces. The magnitude of the d-band center shift for Pt in the PtM alloys ranges from 0.3-0.6 eV for the Ni alloys and 0.4-0.8 eV for the Fe alloys. The d-band center shifts for the Pt in these PtM and PtM_3 alloys are very similar to those of the Pt in the Pt/M/Pt sandwich alloys (d-band center shift of ~0.2 eV or ~0.4 eV when M is Ni or Fe, respectively)[21] and the Pd in the Pd/Fe/Pd sandwich alloy (d-band center shift of 0.5 eV away from the Fermi level)[10]. The similarities in the changes to the Pt d-band between these various surfaces suggest that similar electronic interactions occur between the Ni

or Fe and the Pt atoms; namely, the overlap in the d-states of the Pt atoms with the d-states of the Ni or Fe atoms causes a rehybridization of the Pt's d-states which results in the observed shift in the Pt's d-band center away from the Fermi level.[48] From the previous studies, it is clear that the shift in the d-band center of the surface Pt away from the Fermi level will be accompanied by a deactivation of the surface for molecular adsorption. Second, the increase in the surface coverage of Pt results in a larger shift in the surface Pt's d-band covered surface. For the PtM (111) surfaces, the Pt d-band center shifts from 0.3 eV on the 50% Ni covered surface to 0.6 eV for the 0% Ni covered surface while the shifts are 0.4 eV and 0.8 eV for the respective Fe surfaces. For the PtM_3 (111) surfaces, the Pt d-band shift increases from 0.4 eV for the 75% Ni covered surface to 0.6 eV for the 50% Ni covered surface while the shifts for the Fe surfaces are 0.5 eV to 0.7 eV, respectively. These results suggest that as the surface concentration of Pt increases, the surface will become more strongly deactivated for surface adsorption. Third, the shifts in the surface Pt's d-band center for the various surfaces are larger for the Fe alloys as compared to the Ni alloys. This is clearly seen in Table 3 as the Pt d-band centers for the Fe alloys are all shifted to lower energies compared to the Ni alloys and the Pt d-band widths are larger for the Fe alloys as compared to the Ni alloys which agrees with the results for the Pt/M/Pt sandwich alloys[21]. These results suggest that Fe has a greater degree of interaction with Pt than does the Ni, which likely results in a greater deactivation of the surface Pt for adsorption on the Fe alloy surfaces compared to the Ni alloy surfaces.

As for the base metal component (Ni or Fe) of the PtM and PtM_3 (111) surfaces, an examination of the d-band parameters shows two significant results. First, the hybridization between the M and Pt d-states shifts the Fe's d-states to lower energies (away from the Fermi level) while the Ni's d-states are shifted to higher energies (towards the Fermi level). This shift

of the M species' d-states is larger for the surface Fe, in the range of 0.2-0.5 eV, than for the surface Ni, in the range of 0.1-0.2 eV. These results suggest that the Pt-Fe interactions cause the surface Fe to become less active for molecular adsorption while the Pt-Ni interactions cause the surface Ni to become more active for molecular adsorption. Furthermore, the shift in the Fe's d-band to lower energies in the PtFe and $PtFe_3$ (111) surfaces is similar to that seen in the non-segregated PdFe and Pd_3Fe (111) surfaces, where the d-band center for the PdFe and Pd_3Fe (111) surfaces are -2.58 eV and -2.69 eV, respectively. This change in the Fe's electronic structure in the alloys is different than that observed when the Pd is placed in a patch on the Fe surface as the Fe is only minimally effected by the Pd's presence.[10] These results suggest that the formation of an alloy between Fe and the noble metal (Pd or Pt) is less favorable with respect to the adsorption activity of the bimetallic Fe based surfaces as compared to noble metal patches on the Fe surface. However, even the less active surface Fe in the PtM and PtM_3 alloys has a d-band closer to the Fermi level than the surface Pt. Second, the PtM (111) surfaces have a larger degree of Pt-M interaction, characterized by the shifts in the Pt species' d-band centers, compared to the PtM_3 (111) surfaces. This result shows that the greater the number of Pt-M interactions for a given M atom, the greater the effect of the Pt-M interactions on the M species' d-band structure.

Overall, these results show that the PtM and PtM_3 (111) surfaces will form surface structures with an increased coverage of Pt as compared to the non-segregated structures under vacuum. For the PtM (111) surface, the Pt/M/PtM surface structure (100% Pt coverage) for both Fe and Ni is more energetically favorable than the non-segregated structure (PtM) while the $Pt_3M/PtM_3/PtM$ surface structure (75% Pt coverage) is also energetically favorable for the PtNi alloy. For the PtM_3 (111) surface, the $PtM/M/PtM_3$ surface structure (50% Pt coverage) is the only surface structure which is more energetically favorable than the non-segregated structure

(PtM_3) for both the Ni and Fe alloys. These results differ from the previous studies of Pt_3M alloy (111) surfaces by showing that significantly decreasing the Pt concentration of the alloys leads to more mixed surfaces, over a complete Pt surface layer, and that double Pt layers or double PtM layers are highly unfavorable. The electronic analyses of these surfaces show that the Pt-M interactions cause a hybridization of both the Pt and M species d-states. In the cases of the surface Pt and Fe species, this hybridization causes the metals' d-states to shift to lower energies, away from the Fermi level, which decreases these metals' ability to adsorb molecules. As for the surface Ni species, the Pt-Ni hybridization slightly shifts the Ni's d-states to higher energies, towards the Fermi level, which increases Ni's ability to adsorb molecules.

3.2 Surface Structure Effect on Aromatic Adsorption

3.2.1 Benzene Adsorption

For benzene's adsorption, we examined all possible adsorption sites for the aromatic ring in the bridge 30^o ($B30^o$) and hcp 0^o ($H0^o$) sites (Figures S1 and S2). On the monometallic surface, benzene has eight different adsorption sites. The $B30^o$ site was the most favorable on Pt (111)[49, 50] and Ni (111)[51] and the $H0^o$ site is the second most favorable adsorption site on Pt (111) [49, 50] and is only slightly less favorable than the fcc 0^o ($F0^o$) site on Ni (111)[51]. Due to the increased complexity of the bimetallic surfaces, the number of possible benzene adsorption sites significantly increases as the orientation of the benzene ring becomes dependent upon its position relative to both the surface and subsurface composition. Additionally, previous work by Sabbe, et al.[16] has shown that the $F0^o$ sites for benzene remains less favorable than the $H0^o$ and $B30^o$ sites for Pt_3M surfaces. Based upon the adsorption site preferences for benzene on the Pt (111) and Ni (111) surfaces and previous work on bimetallic alloy surfaces, we have limited our examination of benzene's adsorption to the $B30^o$ and $H0^o$ sites and have varied the adsorbate's

position relative to the surface and subsurface composition in order to gain valuable insight into the surface composition effect on benzene's adsorption without prohibitively increasing the computational cost. The most favorable adsorption site for benzene on each surface studied is shown in Figure 3 while the energetic results from these studies are presented in Table 4. The molecular structure results (e.g. bond lengths and angles within the benzene adsorbate) support the conclusions made from the adsorption and distortion energy results and are shown in the Supporting Information in Tables S1 and S2. Finally, Table 2 shows the segregation energy for the bimetallic surfaces in the presence of a benzene adsorbate which show no significant change in the segregation trend observed with no adsorbate.

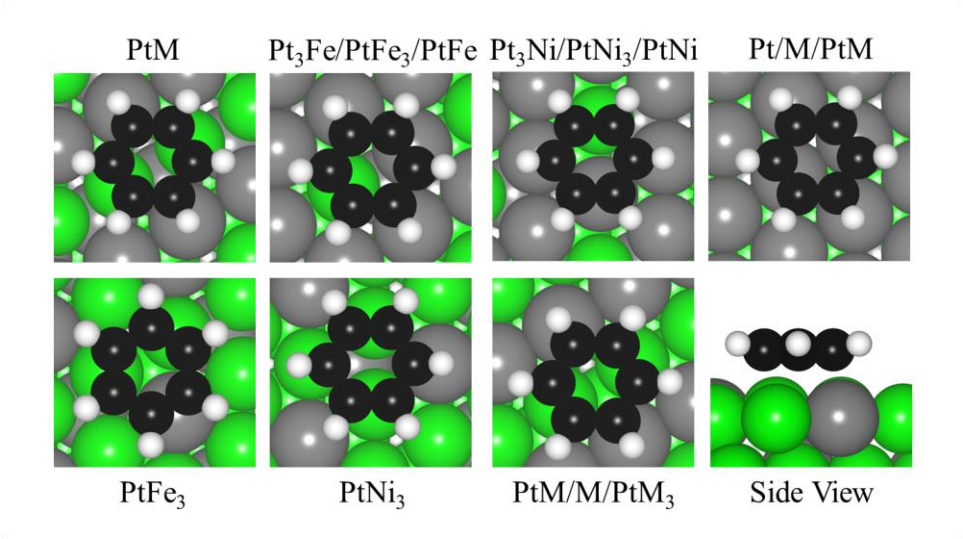

Figure 3. Adsorption sites for benzene on the three most stable PtM (111) surfaces and two most stable PtM_3 (111) surfaces. The surface sphere coloring is identical to that in Figure 1 and the black, white, and red spheres represent carbon, hydrogen, and oxygen, respectively.

On the PtM (111) surface (Figure 3), benzene's adsorption is most favorable on the B30^{o}-MM site for both the PtFe and PtNi surfaces with benzene adsorbing stronger and distorting more on the PtNi (111) surface than the PtFe (111) surface. This is consistent with the d-band parameter results which showed that both the Pt and Ni species in the PtNi (111) surface have d-

band centers nearer the Fermi level than the corresponding Pt and Fe species in the PtFe (111) surface (Table 3).

Table 4. Adsorption energy (E_{ads}) and distortion (E_{dist}) energy for the most favorable adsorption site for benzene on the three most stable PtM (111) surfaces and two most stable PtM_3 (111) surfaces (M = Fe, Ni) in the B30° and H0° configurations with the optB88-vdW functional.[a]

Surface	Site	Eads (eV)	Edist (eV)
PtFe	B30°-FeFe	-1.22	0.87
PtNi	B30°-NiNi	-1.62	1.24
$Pt_3Fe/PtFe_3/PtFe$	B30°-$FePt_{Pt}$	-0.90	0.02
$Pt_3Ni/PtNi_3/PtNi$	B30°-$NiPt_{Ni}$	-1.01	1.18
Pt/Fe/PtFe	B30°	-0.85	0.01
Pt/Ni/PtNi	B30°	-0.86	0.01
$PtFe_3$	H0°-FeFeFe	-1.37	0.80
$PtNi_3$	B30°-$NiNi_{Pt}$	-1.59	1.05
$PtFe/Fe/PtFe_3$	B30°-FeFe	-0.86	0.01
$PtNi/Ni/PtNi_3$	B30°-NiNi	-0.90	1.04

Benzene on Pt (111) and Fe (110) has an E_{ads} of -2.14 eV[52] and -1.97 eV[10], respectively, with the optB88-vdW functional.

Increasing the surface Pt concentration to 75% with the $Pt_3M/PtM_3/PtM$ (111) surface (Figure 3), it is clear that both the adsorption strength and molecular distortion of benzene decrease for both M species (Ni and Fe). On the $Pt_3Fe/PtFe_3/PtFe$ (111) surface, benzene's adsorption energy is most favorable on the B30°-FePtPt site and decreases by ~0.3 eV to -0.90 eV as compared to the PtFe (111) surface. Also, benzene's distortion energy decreases to near zero. The adsorption of benzene on $Pt_3Ni/PtNi_3/PtNi$ (111) is most favorable on the B30°-NiPtNi site and also shows a decrease in adsorption energy of ~0.6 eV to -1.01 eV relative to the PtNi (111) surface. However, the distortion energy only decreases by 0.06 eV to 1.18 eV from the PtNi (111) surface which shows that benzene remains geometrically distorted on the $Pt_3Ni/PtNi_3/PtNi$ (111) surface. Similar to the PtM (111) surface, the Ni alloy surface adsorbs benzene stronger than the Fe alloy surface, which is consistent with the d-band center results for the different alloy surfaces (Table 3). Finally, the overall shift in the Pt, Ni, and Fe surface

species' d-band center to lower energies in the $Pt_3M/PtM_3/PtM$ (111) surfaces as compared to the PtM (111) surfaces is consistent with the weakened adsorption of benzene on the $Pt_3M/PtM_3/PtM$ (111) surfaces.

Further increasing the surface Pt concentration to 100% (Pt/M/PtM (111) surface, Figure 3) shows that there is a decrease in the adsorption energy and distortion of the benzene adsorbate on the Ni alloy surface while the Fe alloy surface results are similar to that seen for the $Pt_3Fe/PtFe_3/PtFe$ (111) surface. For both the Ni and Fe alloys, benzene adsorbs most favorably on the $B30^o$ site on the Pt/M/PtM (111) surface with similar adsorption energies and minimal ring distortion. This is consistent with the large shift in the surface Pt's d-band center away from the Fermi level in both the Fe and Ni alloys (Table 3). When increasing the surface Pt concentration from 75% to 100% ($Pt_3M/PtM_3/PtM$ to Pt/M/PtM), benzene's adsorption on both the Fe and Ni alloy surfaces decreases by only ~0.05 eV; however, benzene's distortion energy decreases by ~1 eV on the Ni surfaces while remaining constant on the Fe surfaces. This result suggests that there is a distinct switch in the adsorption characteristics for benzene on the PtFe (111) surfaces with a surface coverage of 75% Pt while the switch occurs at 100% Pt on the PtNi (111) surfaces.

For benzene's adsorption on the PtM_3 (111) surface (Figure 3), the $B30^o$ -NiNiPt site is the most favorable adsorption site for the $PtNi_3$ (111) surface while the $H0^o$-FeFeFe site is the most favorable adsorption site for the $PtFe_3$ (111) surface. Similar to the PtM (111) surfaces, benzene adsorbs stronger and distorts to a greater degree on the Ni alloy surface than the Fe alloy surface, which is consistent with the d-band parameter results (Table 3). Furthermore, similarity in benzene's adsorption strength on the $PtNi_3$ and PtNi (111) surfaces is likely to do the compensation between the surface Ni concentration and the d-band parameters of the surface

species, with $PtNi_3$ (111) having a higher surface M concentration and a more negative d-band center for the surface Pt as compared to PtNi (111). Similarly, for benzene on the $PtFe_3$ (111) surface as compared to the PtFe (111) surface, the ~0.1 eV change in adsorption energy likely results from the shift in the surface Fe's d-band center by ~0.3 eV towards the Fermi level, as well as the higher Fe surface concentration, for $PtFe_3$ (111) relative to PtFe (111).

Increasing the surface Pt concentration to 50% with the $PtM/M/PtM_3$ (111) surface (Figure 3), it is clear that both the adsorption strength and molecular distortion decrease for benzene's adsorption on the Fe alloys while only benzene's adsorption strength decreases on the Ni alloys. On the $PtFe/Fe/PtFe_3$ (111) surface, benzene's adsorption energy is most favorable on the B30^o-FeFe site and decreases by ~0.5 eV to -0.86 eV compared to the $PtFe_3$ (111) surface. Also, benzene's distortion energy decreases to a near zero value, which suggests a significant weakening of the surface to benzene interactions. The adsorption of benzene on $PtNi/Ni/PtNi_3$ (111) is most favorable on the B30^o-NiNi site and also shows a decrease in adsorption energy by ~0.7 eV to -0.90 eV relative to the $PtNi_3$ (111) surface. However, the distortion energy only decreases by 0.01 eV for benzene on the $PtNi/Ni/PtNi_3$ (111) surface relative to the $PtNi_3$ (111) surface which shows that benzene continues to interact strongly with the $PtNi/Ni/PtNi_3$ (111) surface. Similar to the PtM_3 (111) surface, the Ni alloy surface adsorbs benzene stronger than the Fe alloy surface, which is consistent with the trend in the surface d-band parameters (Table 3). This result suggests that there is a distinct switch in the adsorption characteristics for benzene on the $PtFe_3$ (111) surfaces with a surface coverage of 50% Pt while the no such switch occurs on the $PtNi_3$ (111) surfaces.

Benzene's adsorption on the alloy surfaces is significantly weaker than benzene's adsorption on the pure Pt (111)[53] and pure Fe (110)[10] surfaces using the optB88-vdW functional

(Table 4). Compared to the Pt (111) surface, benzene's adsorption on the most favorable of the PtM and PtM_3 (111) surfaces (PtNi) is ~0.5 eV weaker (Table 4). While benzene's adsorption on the pure Fe (110) surface is nearly -2 eV[10], adsorption on the most favorable PtFe and $PtFe_3$ (111) surfaces shows that the presence of the second metal (Pt) decreases benzene's adsorption energy by ~0.8 eV and ~0.6 eV, respectively. Comparison of the above adsorption energy results with the adsorption energy of benzene on Ni (111) could not be made as no research group yet has investigated benzene's adsorption on said surface with the optB88-vdW functional.

Comparing the adsorption strength of benzene with the barrier for C-O cleavage on monometallic surfaces shows that these reactions likely compete for the rate limiting step, suggesting that the weakening of benzene's adsorption on the Pt/Fe and Pt/Ni surfaces relative to the monometallic surfaces contributes to the improved HDO performance of these bimetallic catalysts. From our previous work on the monometallic, Fe (110) surface, the desorption energy of benzene (the desired product of the HDO of phenol) is similar to the activation energy for the cleavage of the C-O bond.[10, 54] In fact, for the most favorable mechanism for the HDO of phenol on Fe (110), the barriers for breaking the C-O bond and desorbing benzene were 1.04 eV and 1.21/1.97 eV (without/with van der Waals corrections);[10, 54] this suggests that this complex reaction has multiple rate limiting steps, each with their own, potentially significant degree of rate control[55-57]. Furthermore, studies for the HDO of guaiacol and phenol on Pt (111) show that the barriers for cleaving the C-O bond can range from 0.6-2.4 eV depending on the surface structure of the phenolic molecule.[58, 59] As shown by Nie, et al.,[6] the likely mechanism for C-O cleavage for *m*-cresol on Pt catalysts involves the partial hydrogenation of the phenolic molecule via its tautomerization, which is predicted to reduce the barrier for C-O cleavage of phenol on Pt (111) from ~2.3 eV to ~1.1 eV. Comparing these energy barrier results for C-O cleavage in

phenolics to the desorption energy of the wanted benzene product (1.3/2.1 eV without/with van der Waals corrections)[16, 50, 52], it is clear that both the desorption of benzene and cleavage of the C-O bond likely compete as the rate limiting steps, each with the potential to have non-zero degrees of rate control[55-57]. Additionally, the same trend observed above for the Fe (110) and Pt (111) surfaces remain true for the Ru (0001) surface, suggesting that the observed competition between benzene desorption and C-O cleavage extends to other surfaces.[60] Qualitatively applying the logic behind the idea of the degree of rate control to this system,[55-57] the decrease in the adsorption energy of benzene on the PtM and PtM_3 alloy surfaces as compared to the pure metal surfaces will likely enhance the overall rate of reaction for the HDO of phenol by decreasing the degree of rate control for the desorption of the wanted HDO product (benzene), subsequently increasing the catalyst's turnover frequency.

The weakened adsorption of benzene on Pt/Fe and Pt/Ni surfaces compared to the Pt (111) surface observed here is consistent with previous experimental work on PtSn (111) surfaces. The temperature programmed desorption (TPD) of benzene was studied by Koel, et al.[61, 62] on Pt (111) and PtSn (111) surfaces. These studies show that benzene does not desorb from Pt (111) at low coverages, but instead decomposes to adsorbed carbon with desorbed H_2 in the range of 400-725 K. Additionally, increasing the coverage of benzene on the surface shows that benzene desorption peaks appear in the range of 178-480 K; however, the decomposition of adsorbed benzene to adsorbed carbon and desorbed H_2 remains in the previously mentioned temperature range. These results show that, on Pt (111), there is a strong competition between benzene's desorption and further decomposition. Even at the higher coverages where benzene is seen to desorb, there is an overlap between the benzene desorption temperatures and the temperatures at which benzene decomposes to H_2. Therefore, despite the HDO reaction often

being conducted at 575 K[6, 8, 63], the desorption of the wanted product, benzene, without its further decomposition likely competes for the rate limiting step with C-O cleavage on Pt (111). This is further supported by a theoretical study of the dehydrogenation of benzene on Pt (111) which showed that the first two dehydrogenation steps for benzene on Pt (111) have barriers in the range of 0.76-1.72 eV,[64] which is lower than the desorption barrier for benzene on Pt (111) with van der Waals corrections[52, 53, 59]. Furthermore, the desorption of benzene from the PtSn (111) alloy surfaces show that the addition of the second metal (Sn) to the Pt (111) surface results in the desorption of benzene at lower temperatures (~170-350 K at all coverages) and subsequently prevents the decomposition of benzene to H_2. This weakening of benzene's adsorption on the PtSn (111) surfaces compared to the Pt (111) surface is similar to the behavior noted here on the Pt/Fe and Pt/Ni surfaces. Overall, these results suggest that the reduced desorption barrier for the wanted HDO product, benzene, on the Pt/Fe and Pt/Ni surfaces likely contributes to the improved HDO activity of said surfaces is supported by the provided surface science studies on Pt (111) and PtSn (111) surfaces.

In order to further characterize the surface to adsorbate electronic interactions occurring between benzene and the PtM and PtM_3 (111) surfaces, we have calculated the differential charge density (Equation 6) for benzene in the most favorable adsorption site on each of the surfaces studied for benzene adsorption. In addition to the differential charge density distributions shown in Figure 4, we have also quantified the mean charge displacement upon benzene's adsorption onto each site (Equation 7) and the results are shown in Table 5. Our previous work has shown that the trends in both the differential charge density and mean charge displacement (Q) are consistent with changes observed in the density of states,[10, 65] and we

believe that these two analyses can be used to quantify the electronic interactions between adsorbate and surface.

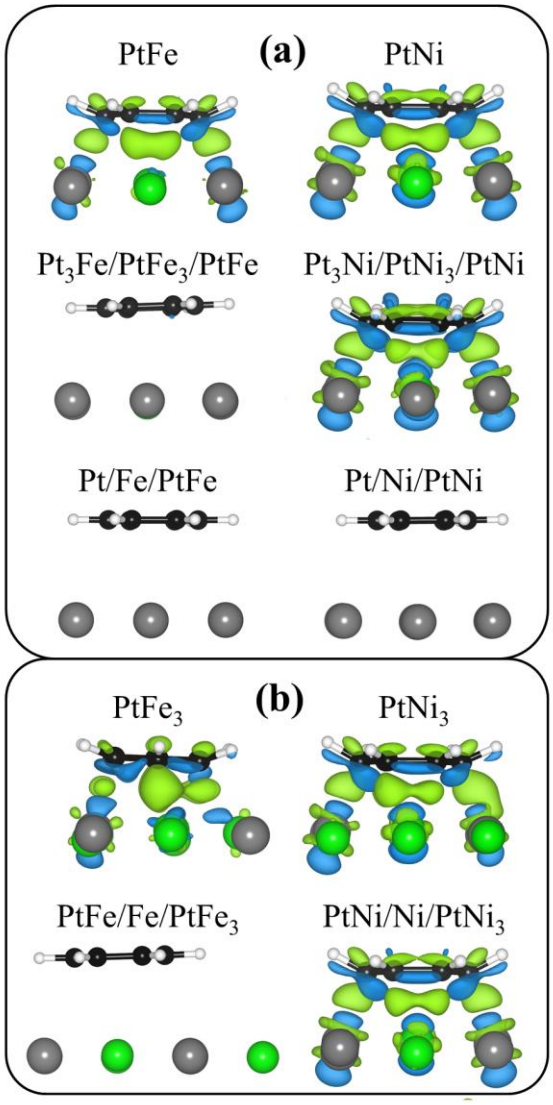

Figure 4. Differential charge density distributions for benzene in its most favorable adsorption sites on the (a) PtM (111) surfaces and the (b) PtM_3 (111) surfaces. The surface sphere coloring is identical to that in Figure 1 and the black and white spheres represent carbon and hydrogen, respectively. The isosurface level was set to 0.005 electrons/$Bohr^3$ and the green and blue areas represent a gain and loss of electrons. The calculations were performed using the optB88-vdW functional.

Table 5. Mean charge displacement (Q) upon benzene's and phenol's adsorption on the PtM and PtM_3 (111) surface structures (M = Fe, Ni) with the optB88-vdW functional. Phenol's horizontal, vertical atop M species, and vertical atop Pt species adsorption sites are denoted as H, V-M, and V-Pt, respectively.

Surface	Benzene	Phenol		
	Q (electrons)	H Q (electrons)	V-M Q (electrons)	V-Pt Q (electrons)
PtFe	1.24	1.30	0.47	0.41
PtNi	1.54	1.59	0.48	0.39
$Pt_3Fe/PtFe_3/PtFe$	0.44	0.45	0.39	0.31
$Pt_3Ni/PtNi_3/PtNi$	1.60	1.62	0.42	0.35
Pt/Fe/PtFe	0.33	0.38	-	0.27
Pt/Ni/PtNi	0.36	0.42	-	0.28
$PtFe_3$	1.23	-	0.48	0.38
$PtNi_3$	1.42	1.48	0.50	0.34
$PtFe/Fe/PtFe_3$	0.40	0.56	0.82	0.30
$PtNi/Ni/PtNi_3$	1.43	1.45	0.43	0.29

From the differential charge density distributions, it is clear that benzene is chemisorbed on the PtFe, PtNi, $Pt_3Ni/PtNi_3/PtNi$, $PtFe_3$, $PtNi_3$, and $PtNi/Ni/PtNi_3$ (111) surfaces while benzene is physisorbed on the $Pt_3Fe/PtFe_3/PtFe$, Pt/Fe/PtFe, Pt/Ni/PtNi, and $PtFe/Fe/PtFe_3$ (111) surfaces. This is based on the large degree of charge transfer seen between the benzene adsorbate and bimetallic surfaces for the chemisorbed systems, along with the negligible amount of charge transfer seen between the benzene adsorbates and bimetallic surfaces for the physisorbed systems (Figure 4). This difference in adsorption strength can also be seen in the mean charge displacement, which is greater than 1 electron for the chemisorbed systems and less than 0.5 electrons for the physisorbed systems (Table 5), and the distortion energy for the benzene adsorbate, which is greater than 1 eV for the chemisorbed systems and negligible for the physisorbed systems (Table 4). Furthermore, it is clear from both the differential charge density and the mean charge displacement results that the Ni alloys have a greater degree of electronic interactions with the adsorbing benzene with the Ni surfaces exchanging an average of 0.2-0.3

electrons more with the adsorbing benzene in the chemisorbed systems (PtM and PtM_3 surface structures) than the Fe alloys. However, as a portion of the surface in each case is covered in electronically deactivated Pt, the mean charge displacement between benzene and the Ni alloy surfaces is 0.5-0.7 electrons less than that seen for benzene adsorbed on Ni (111) using the PBE functional.[47] This weakening in the charge transfer between surface and adsorbate for benzene on the bimetallic surfaces is consistent with our analysis of the bimetallic surfaces' d-band structure and the weakening of the adsorption energy of benzene on these bimetallic surfaces.

3.2.2 Phenol Adsorption

The adsorption of phenol was studied on the three most favorable PtM (111) surfaces (PtM, $Pt_3M/PtM_3/PtM$, and Pt/M/PtM as shown in Figure 1A, 1B, and 1C, respectively) and the two most favorable PtM_3 (111) surfaces (PtM_3 and $PtM/M/PtM_3$ as shown in Figure 2A and 2B, respectively), similar to benzene's adsorption. Due to the addition of the hydroxyl functional group on the aromatic ring, the total number of possible phenol adsorption sites on the model (111) surfaces significantly increases as both the horizontal adsorption sites (via the aromatic ring) must account for the hydroxyl position above the surface and the hydroxyl group introduces new vertical adsorption sites (via only the hydroxyl group). On the monometallic (111) surface, phenol has been shown to have 26 separate horizontal adsorption sites[65] with the $B30^o$ ring site with the hydroxyl group above a surface bridge site being the most favorable on Pt (111),[66] Rh (111),[66] and Pd (111)[65, 67] while the hydroxyl group prefers a top site for phenol's adsorption on Ni (111)[68]. The increased complexity of the bimetallic surfaces studied here will significantly increase the number of possible phenol adsorption sites as both the orientation of the aromatic ring and the hydroxyl group above the surface becomes dependent upon their relative position to both the surface and subsurface composition. In order to simplify the models and gain a useful

understanding of phenol's interaction with the PtM and PtM_3 (111) surfaces, we have limited our examination of phenol's adsorption to the most favorable benzene adsorption sites on the PtM and PtM_3 (111) surfaces (section 3.2.1) with the hydroxyl group placed above the bridge site, as was found to be the most favorable hydroxyl site on Pt (111)[66] and Pd (111)[65, 67], and the most favorable vertical adsorption site (top-bridge) for phenol on Pd (111)[65] with the hydroxyl group placed atop both a surface M species and surface Pt species where possible. The reasoning for the vertical adsorption choice is that only on Pd (111)[65] has the possible phenol vertical adsorption sites been presented and their relative stabilities show that there is no significant change in adsorption energy with a change in adsorption site, which suggests that the result obtained with the chosen vertical adsorption site will be extendable onto other vertical adsorption sites. Finally, placing the hydroxyl atop a surface atom in the vertical phenol adsorption site allowed us to better directly characterize the Pt-O and M-O interactions. The sites studied for phenol on the model PtM (111) and PtM_3 (111) surfaces are shown in Figure 5 while the energetic results from these studies are presented in Table 6. The molecular structure results (e.g. bond lengths and angles within the benzene adsorbate) support the conclusions made from the adsorption and distortion energy results and are shown in the Supporting Information in Table S3. Finally, Table 2 shows the segregation energy of the bimetallic surfaces studied here in the presence of a phenol adsorbate which results in no significant change to the segregation trend observed with no adsorbate.

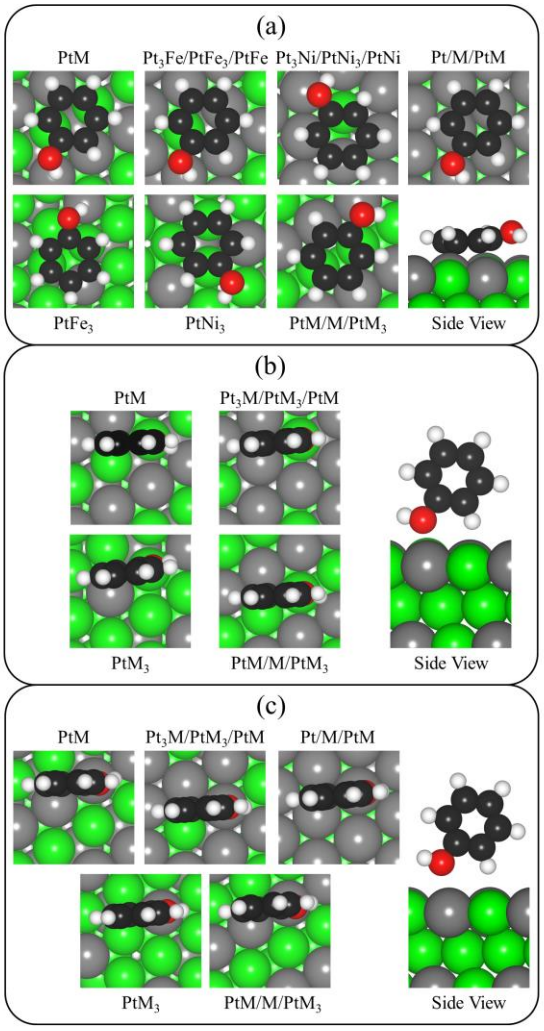

Figure 5. Adsorption sites for phenol on the three most favorable PtM (111) surfaces and the two most favorable PtM_3 (111) surfaces. The horizontal adsorption sites (a), vertical adsorption sites atop a surface M species (b), and vertical adsorption sites atop a surface Pt species (c) are shown. The surface sphere coloring is identical to that in Figure 1 and the black, red, and white spheres represent carbon, oxygen, and hydrogen, respectively.

Table 6. Adsorption energy (E_{ads}) and distortion (E_{dist}) energy for phenol adsorbed on the three most stable PtM (111) surfaces and two most stable PtM_3 (111) surfaces (M = Fe, Ni). Both

horizontal and vertical adsorption sites are shown and the calculations were performed with the optB88-vdW (PBE) functional.

Surface	Horizontal Sites		Vertical Sites - M		Vertical Sites - Pt	
	E_{ads} (eV)	E_{dist} (eV)	E_{ads} (eV)	E_{dist} (eV)	E_{ads} (eV)	E_{dist} (eV)
PtFe	-1.29	1.10	-0.73	0.04	-0.46	0.02
PtNi	-1.66 (-0.75)	1.39	-0.66	0.02	-0.47	0.01
$Pt_3Fe/PtFe_3/PtFe$	-1.02	0.02	-0.69	0.01	-0.45	0.00
$Pt_3Ni/PtNi_3/PtNi$	-1.03	1.22	-0.61	0.01	-0.48 (-0.03)	0.01
Pt/Fe/PtFe	-1.00	0.01	-		-0.46	0.00
Pt/Ni/PtNi	-1.00	0.01	-		-0.46	0.00
$PtFe_3$	Unstable		-0.78 (-0.28)	0.02	-0.40	0.00
$PtNi_3$	-1.62	1.11	-0.61	0.02	-0.45	0.00
$PtFe/Fe/PtFe_3$	-1.05	0.05	-0.68	0.02	-0.43	0.00
$PtNi/Ni/PtNi_3$	-0.92	1.09	-0.54	0.01	-0.44	0.00

Phenol on Pd (111) and Fe (110) has an E_{ads} of -2.23 eV and -1.99 eV, respectively, with the optB88-vdW functional.[65]

For phenol's horizontal adsorption on the PtM and PtM_3 (111) surfaces (Figure 5a), the trend in the adsorption and distortion energies is similar to that observed for benzene's adsorption. The adsorption energy for the strongest horizontal phenol adsorption site, PtNi (111), was calculated without van der Waals corrections (via the PBE functional) and was found to be -0.75 eV which shows that the van der Waals corrections increased the adsorption energy of horizontal phenol by 0.9 eV, similar to that seen in our previous work on Fe (110).[10] Compared to benzene's adsorption, phenol adsorbs slightly stronger and has a slightly higher distortion energy for all surfaces examined. Additionally, the trends observed for benzene adsorption with respect to the surface composition are identical for phenol which shows that the addition of the hydroxyl functional group to the aromatic ring does not significantly affect the interactions occurring between the aromatic ring and the surface. Overall, these results show that the addition of the hydroxyl functional group does not significantly alter the adsorption of the aromatic ring, with the trends in phenol's adsorption following closely the trends in benzene's adsorption on the

PtM and PtM_3 (111) surfaces, and that the C-O bond is not significantly altered by the surface-adsorbate interactions.

Phenol's vertical adsorption on the PtM and PtM_3 (111) surfaces (Figure 5b and 5c) is similar to that seen on the Pd (111) surface[65] with phenol only weakly adsorbing to the metal surface through the hydroxyl functional group with adsorption energies ranging from -0.40 eV to -0.78 eV and distortion energies near zero (Table 6). The weakness of phenol's vertical adsorption is further confirmed by calculating the adsorption energies of the strongest sites for the V-M and V-Pt configurations ($PtFe_3$ and $Pt_3Ni/PtNi_3/PtNi$, respectively) without van der Waals corrections (via the PBE functional), which were found to be -0.28 eV and -0.03 eV, respectively. For phenol adsorbed vertically atop a surface M species, the adsorption energies range from -0.54 eV to -0.78 eV with phenol adsorbing stronger on the Fe alloy surfaces as compared to the Ni alloy surfaces. This is a significant change in the observed trend for benzene and horizontally adsorbed phenol and shows that the Fe-O interaction is stronger than the Ni-O interaction, suggesting that the Fe surfaces would be more likely to break the C-O bond in phenol. While the horizontal adsorption sites showed a significant decrease in adsorption energy as the Pt surface concentration increased, the vertical M sites adsorption energy only decreases by ~0.1 eV as the surface Pt concentration increases, which is consistent with the vertical sites being physisorbed. For phenol adsorbed vertically atop a surface Pt species, the adsorption energies are nearly identical on all surfaces (Table 6) which suggests that the Pt-O interaction is weaker than the M-O interactions. Overall, these results show that the vertical phenol sites only weakly binds to the bimetallic surfaces, with higher M species concentration have a slightly stronger adsorption energy for vertical phenol atop surface M species and that the Fe alloy surfaces bind vertical phenol stronger than the Ni alloy surfaces.

Thus far, phenol's adsorption on monometallic surfaces with the optB88-vdW functional has been limited to the pure Pd (111)[65] and pure Fe (110)[65] surfaces. For the horizontal structures, phenol adsorbs significantly weaker on the PtM and PtM_3 (111) surfaces compared to both the Pd (111) and Fe (110) surfaces (Table 6). Overall, the comparison of the adsorption strength of phenol on the bimetallic surfaces studied here to related monometallic surfaces has a similar result to that of benzene.

In order to characterize the surface to adsorbate electronic interactions occurring between phenol and the PtM and PtM_3 (111) surfaces, we have calculated the differential charge density (Equation 6) for phenol in each of the stable sites studied for phenol adsorption (Figure S3). Additionally, we have quantified the mean charge displacement upon phenol's adsorption onto each site (Equation 7) and the results are shown in Table 5.

For the adsorption of phenol PtM and PtM_3 (111) model surfaces, both the differential charge density (Figure S3) and mean charge displacement (Table 5) results show that phenol's adsorption has a similar electronic trend to that of benzene on these surfaces. The only significant difference between the benzene's and phenol's adsorption is in the charge transfer between the hydroxyl group and the bimetallic surface. For the horizontal phenol adsorption sites, the presence of the hydroxyl functional group in the phenol adsorbate does not significantly alter the surface-adsorbate interactions for the aromatic species and the PtM and PtM_3 (111) surfaces, due to the similarity between the benzene and horizontal phenol differential charge density distribution and mean charge displacement results. The only significant difference is in the differential charge density results for the chemisorbed systems (PtFe, PtNi, $Pt_3Ni/PtNi_3/PtNi$, $PtNi_3$, and $PtNi/Ni/PtNi_3$) which show that there is a small degree of charge exchange between the surface and the hydrogen within the hydroxyl group. This charge exchange is similar to that

seen for phenol on Pd (111)[65] and suggests that these surfaces could easily deprotonate the hydroxyl group upon phenol's adsorption, as shown for other phenolic compounds on Pd (111)[69, 70] and phenol on Pt (111)[71]. For the vertical adsorption sites, it is clear that there are only minor changes to the amount of charge transferred upon phenol's adsorption with a change in the surface composition and that the charge transferred for the Ni alloys is similar to that seen for the Fe alloys. This is consistent with the adsorption and distortion energy results showing that the vertical sites are likely physisorbed. Comparing the vertical M sites to the vertical Pt sites shows that the larger adsorption energy for phenol on the vertical M sites is due to the increased charge transferred between the surface and adsorbate of ~0.1 electrons. Overall, the vertical site electronic interactions show that the decreased adsorption energy of these sites relative to the horizontal sites is due to a decrease in the charge transferred between the surface and adsorbate and that the charge exchange between the oxygen and surface causes a loss of electrons in the C-O bond which weakens the bond and causes it to lengthen, as seen in the geometric results in Table S3.

3.2.3 Effect of Surface and Subsurface Composition on Aromatic Adsorption

Here, we examined the effect of the surface and subsurface composition on the adsorption of aromatic compounds on the PtM and PtM_3 (111) surfaces. For the surface composition comparisons, the PtM/M/PtM_3 and Pt/M/PtM (111) surfaces were examined, along with the Pt_3M/PtM_3/PtM and PtM_3 (111) surfaces. These surfaces were chosen as they have differing surface compositions with similar subsurface compositions. For the subsurface composition comparisons, the PtM and PtM/M/PtM_3 (111) surfaces were examined as these surfaces have similar surface layers with different subsurface compositions.

A comparison of the two sets of surfaces with similar subsurface compositions ($PtM/M/PtM_3$ to Pt/M/PtM and $Pt_3M/PtM_3/PtM$ to PtM_3) was made to determine the effect of the surface structure on the adsorption of aromatics. For the $PtM/M/PtM_3$ and Pt/M/PtM (111) surfaces, aromatic adsorbates are physisorbed on both the Fe and Ni surfaces. This is likely due to the highly negative d-band center for the surface species in these surfaces (Table 3). The only exception is the $PtNi/Ni/PtNi_3$ surface which has a weak adsorption energy (Tables 4 and 6), but still distorts the aromatic adsorbates and shows a strong degree of charge transfer between adsorbate and surface (Table 5). For the $Pt_3M/PtM_3/PtM$ and PtM_3 (111), the aromatic adsorbates are physisorbed on the $Pt_3M/PtM_3/PtM$ surfaces while they are chemisorbed on the PtM_3 surfaces (Tables 4 and 6). Similar to the previous comparison, increasing the surface Pt concentration shifts the d-band center for the surface species further from the Fermi level (Table 3) which corresponds to the weakened adsorption of aromatics. The results from these comparisons show that the adsorption of aromatics on the PtM and PtM_3 surfaces can be tailored by altering the surface composition independent of the subsurface composition. This is similar to the behavior of Pd/Fe surfaces[7, 10] and shows that the ability to tailor aromatic adsorption on base metals by doping with noble metals extends beyond the initially studied Pd/Fe surfaces.

The effect of the subsurface composition on the adsorption of aromatics on the PtM and PtM_3 (111) bimetallic surfaces was determined by examining the PtM and $PtM/M/PtM_3$ (111) surfaces. For both the Fe and Ni alloys, aromatics chemisorb on the PtM surface and physisorb on the $PtM/M/PtM_3$ surfaces. The only exception is the $PtNi/Ni/PtNi_3$ surface which has a weak aromatic adsorption energy, but significantly distorts the aromatic adsorbates. These results show that the adsorption behavior of aromatics on the PtM and PtM_3 surfaces can be tailored by

changing the subsurface layer, which subsequently alters the surface's electronic structure without a change in surface composition.

Overall, our work shows that aromatic adsorption on the PtM and PtM_3 (111) surfaces is more energetically favorable on the near surface structures with higher surface concentrations of the M species. This is consistent with previous work on Pd/Fe surfaces[7, 10] and Pt_3M (111) surfaces[16]. Due to the significant change in the d-band properties of the surface metal species by the Pt-M interactions, even the most favorable PtM and PtM_3 adsorption systems adsorb aromatics to a weaker degree than the comparable monometallic surfaces. The weakened adsorption strength of aromatics on these low concentration Pt alloys relative to the pure metal surfaces suggests that a portion of the improved HDO performance of these bimetallic surfaces is due to the faster desorption of products, leading to a higher turnover rate. Specifically, the weakly chemisorbed states for benzene and phenol on the $Pt_3Ni/PtNi_3/PtNi$ (111) and $PtNi/Ni/PtNi_3$ (111) surfaces show that certain PtNi alloy compositions both significantly distort surface aromatics while having a weak adsorption strength. This balancing of adsorption inactive Pt with adsorption active Ni species in the surface layer creates an ideal situation for the reaction of aromatics, such as the HDO of phenolics[11] or hydrogenation of benzene[72], by reducing the barrier for desorption without losing the surface induced molecular distortion that results in reaction. This work shows that the trends in aromatic adsorption and the tunable surface electronic structure with surface bimetallic composition observed for the Pd/Fe surfaces is extendable to other noble metal/base metal systems.

4. Conclusions

The adsorption of benzene and phenol were studied on the PtM and PtM_3 (111) surfaces, with M being either Ni or Fe. Under vacuum, we found that there is a strong preference for Pt to

surface segregate in each alloy, with a surface of 1 ML and 0.5 ML Pt coverage being the most favorable PtM and PtM_3 (111) surfaces, respectively. A d-band analysis of the surfaces under vacuum showed that the Pt-M interactions shifted the Pt's d-band center to lower energies and increasing the surface Pt concentration shifted the d-band center further from the Fermi level. Also, the Pt-M interactions had a larger effect on the Fe's d-states than the Ni's d-states as the Fe's d-band center was shifted away from the Fermi level while the Ni's d-band center remained largely unchanged, with only a small shift towards the Fermi level. The adsorption of benzene and phenol was found to be significantly stronger on surfaces with higher surface M concentrations. This increase in adsorption strength was found to be due to the greater charge transfer between adsorbate and surface and was likely caused by the higher d-band centers (nearer the Fermi level) for the surface species with higher M concentrations in the surface layer. A comparison of the adsorption of benzene and phenol shows that the addition of the hydroxyl group to the aromatic ring does not significantly affect either the adsorption of the aromatic species on the model surfaces or the surface to adsorbate interactions. Overall, these results show that both benzene and phenol are weakly chemisorbed on several different near surface configurations of Pt/Fe and Pt/Ni alloys and that this adsorption behavior likely contributes to the improved catalytic HDO performance of these types of bimetallic surfaces by reducing the desorption energy of the wanted aromatic products, and thereby increasing the catalyst's turnover frequency. Additionally, this work shows that the electronic and adsorptive behavior observed for the Pd/Fe system is extendable to other noble/base metal systems.

Supporting Information

The details concerning the clean surface species d-band parameters, benzene adsorption sites, geometric parameters for adsorbed benzene and phenol, and differential charge density

distributions for all of the studied phenol adsorption sites are shown in the Supporting Information.

Acknowledgements

This work was supported by institutional funds provided to J.S.M. from the Voiland School of Chemical Engineering and Bioengineering and was partially funded by USDA/NIFA through Hatch Project #WNP00807 titled: "Fundamental and Applied Chemical and Biological Catalysts to Minimize Climate Change, Create a Sustainable Energy Future, and Provide a Safer Food Supply". Our thanks also go to the donors of The American Chemical Society Petroleum Research Fund for partial support of this research. This work was also partially supported by U. S. Department of Energy (DOE), Office of Basic Energy Sciences, Division of Chemical Sciences, Biosciences and Geosciences under Award Numbers DE-SC-0014560 and DE-FG02-05ER15712. Finally, S.S. thanks the Research Internships in Science and Engineering (RISE) program, which is supported by the Federal Republic of Germany through funding from the Federal Ministry of Education and Research.

References

1. M. D. Amiridis, C. Mihut, M. Maciejewski and A. Baiker, *Top. Catal.*, 2004, **28**, 141-150.
2. O. T. Holton and J. W. Stevenson, *Platinum Met. Rev.*, 2013, **57**, 259-271.
3. R. D. Cortright, R. R. Davda and J. A. Dumesic, *Nature*, 2002, **418**, 964-967.
4. J. Zhu, T. Wang, X. Xu, P. Xiao and J. Li, *Appl. Catal. B*, 2013, **130-131**, 197-217.
5. R. Maggi and B. Delmon, *Biomass Bioenergy*, 1994, **7**, 245-249.
6. L. Nie and D. E. Resasco, *J. Catal.*, 2014, **317**, 22-29.
7. J. Sun, A. M. Karim, H. Zhang, L. Kovarik, X. Li, A. J. Hensley, J.-S. McEwen and Y. Wang, *J. Catal.*, 2013, **306**, 47-57.
8. Y. Hong, H. Zhang, J. Sun, A. M. Karim, A. J. Hensley, M. Gu, M. H. Engelhard, J.-S. McEwen and Y. Wang, *ACS Catal.*, 2014, **4**, 3335–3345.
9. R. N. Olcese, M. Bettahar, D. Petitjean, B. Malaman, F. Giovanella and A. Dufour, *Appl. Catal. B*, 2012, **115**, 63-73.
10. A. J. Hensley, R. Zhang, Y. Wang and J.-S. McEwen, *J. Phys. Chem. C*, 2013, **117**, 24317-24328.
11. P. T. M. Do, A. J. Foster, J. Chen and R. F. Lobo, *Green Chem.*, 2012, **14**, 1388-1397.
12. A. V. Ruban, H. L. Skriver and J. K. Nørskov, *Phys. Rev. B*, 1999, **59**, 15990-16000.
13. A. U. Nilekar, A. V. Ruban and M. Mavrikakis, *Surf. Sci.*, 2009, **603**, 91-96.

14. P. Varga, M. Schmid and W. Hofer, *Surf. Rev. Lett.*, 1996, **3**, 1831-1845.
15. Y. Ma and P. B. Balbuena, *Surf. Sci.*, 2008, **602**, 107-113.
16. M. K. Sabbe, L. Lain, M. F. Reyniers and G. B. Marin, *Phys. Chem. Chem. Phys.*, 2013, **15**, 12197-12214.
17. H.-C. Tsai, T. H. Yu, Y. Sha, B. V. Merinov, P.-W. Wu, S.-Y. Chen and W. A. Goddard, *J. Phys. Chem. C*, 2014, **118**, 26703-26712.
18. R. Callejas-Tovar and P. B. Balbuena, *Surf. Sci.*, 2008, **602**, 3531-3539.
19. Y. Gauthier, *Surf. Rev. Lett.*, 1996, **3**, 1663-1689.
20. I. Matanović, F. H. Garzon and N. J. Henson, *J. Phys. Chem. C*, 2011, **115**, 10640-10650.
21. J. R. Kitchin, J. K. Nørskov, M. A. Barteau and J. G. Chen, *J. Chem. Phys.*, 2004, **120**, 10240-10246.
22. B. Hammer and J. K. Nørskov, *Surf. Sci.*, 1995, **343**, 211-220.
23. W. Chen, W. F. Schneider and C. Wolverton, *J. Phys. Chem. C*, 2014, **118**, 8342-8349.
24. H.-Y. Su, X.-K. Gu, X. Ma, Y.-H. Zhao, X.-H. Bao and W.-X. Li, *Catal. Today*, 2011, **165**, 89-95.
25. I. A. Pašti, N. M. Gavrilov and S. V. Mentus, *Electrochim. Acta*, 2014, **130**, 453-463.
26. Y. Ma and P. B. Balbuena, *Surf. Sci.*, 2009, **603**, 349-353.
27. V. A. Bogdanovskaya, M. R. Tarasevich, L. A. Reznikova and L. N. Kuznetsova, *Russ. J. Electrochem.*, 2010, **46**, 1011-1020.
28. V. R. Stamenkovic, B. S. Mun, K. J. J. Mayrhofer, P. N. Ross and N. M. Markovic, *J. Am. Chem. Soc.*, 2006, **128**, 8813-8819.
29. M. Oezaslan, F. Hasché and P. Strasser, *ECS Trans.*, 2011, **41**, 1659-1668.
30. I. Abrikosov, A. Ruban, H. Skriver and B. Johansson, *Phys. Rev. B*, 1994, **50**, 2039-2042.
31. G. Kresse and J. Furthmueller, *Phys. Rev. B*, 1996, **54**, 11169-11186.
32. G. Kresse and J. Hafner, *Phys. Rev. B*, 1993, **47**, 558-561.
33. B. Hammer, L. B. Hansen and J. K. Nørskov, *Phys. Rev. B*, 1999, **59**, 7413-7421.
34. J. P. Perdew, K. Burke and M. Ernzerhof, *Phys. Rev. Lett.*, 1996, **77**, 3865-3868.
35. J. Klimeš, D. R. Bowler and A. Michaelides, *Phys. Rev. B*, 2011, **83**, 195131.
36. J. Klimeš, D. R. Bowler and A. Michaelides, *J. Phys. Condens. Matter*, 2010, **22**, 022201.
37. M. Methfessel and A. T. Paxton, *Phys. Rev. B*, 1989, **40**, 3616-3621.
38. G. Makov and M. C. Payne, *Phys. Rev. B*, 1995, **51**, 4014-4022.
39. H. J. Monkhorst and J. D. Pack, *Phys. Rev. B*, 1976, **13**, 5188-5192.
40. T. Mohri and Y. Chen, *J. Alloy Compd.*, 2004, **383**, 23-31.
41. P. Villars and L. D. Calvert *Pearson's Handbook of Crystallographic Data for Intermetallic Phases*; ASM International: Materials Park, OH, 1991.
42. T. Nimmanwudipong, R. C. Runnebaum, D. E. Block and B. C. Gates, *Catal. Lett.*, 2011, **141**, 779-783.
43. C. A. Menning, H. H. Hwu and J. G. Chen, *J. Phys. Chem. B*, 2006, **110**, 15471-15477.
44. R. Hirschl, F. Delbecq, P. Sautet and J. Hafner, *J. Catal.*, 2003, **217**, 354–366.
45. C. A. Menning and J. G. Chen, *J. Chem. Phys.*, 2009, **130**, 174709.
46. L. Ghiringhelli, R. Caputo and L. Delle Site, *Phys. Rev. B*, 2007, **75**, 113403.
47. L. Delle Site and D. Sebastiani, *Phys. Rev. B*, 2004, **70**, 115401.
48. N. Schweitzer, H. Xin, E. Nikolla, J. T. Miller and S. Linic, *Top. Catal.*, 2010, **53**, 348-356.
49. C. Morin, D. Simon and P. Sautet, *J. Phys. Chem. B*, 2004, **108**, 5653-5665.
50. C. Morin, D. Simon and P. Sautet, *J. Phys. Chem. B*, 2003, **107**, 2995-3002.
51. F. Mittendorfer and J. Hafner, *Surf. Sci.*, 2001, **472**, 133-153.

52. R. Zhang, A. J. Hensley, J.-S. McEwen, S. Wickert, E. Darlatt, K. Fischer, M. Schöppke, R. Denecke, R. Streber, M. Lorenz, C. Papp and H.-P. Steinrück, *Phys. Chem. Chem. Phys.*, 2013, **15**, 20662-20671.
53. W. Liu, J. Carrasco, B. Santra, A. Michaelides, M. Scheffler and A. Tkatchenko, *Phys. Rev. B*, 2012, **86**, 245405.
54. A. J. Hensley, Y. Wang and J.-S. McEwen, *ACS Catal.*, 2015, **5**, 523-536.
55. C. Stegelmann, A. Andreasen and C. T. Campbell, *J. Am. Chem. Soc.*, 2009, **131**, 8077-8082.
56. C. T. Campbell, *J. Catal.*, 2001, **204**, 520-524.
57. C. T. Campbell, *Top. Catal.*, 1994, **1**, 353-366.
58. K. Lee, G. H. Gu, C. A. Mullen, A. A. Boateng and D. G. Vlachos, *ChemSusChem*, 2014, **8**, 315–322.
59. J. Lu, S. Behtash, O. Mamun and A. Heyden, *ACS Catal.*, 2015, **5**, 2423-2435.
60. J. Lu and A. Heyden, *J. Catal.*, 2015, **321**, 39-50.
61. C. Xu, Y.-L. Tsai and B. E. Koel, *J. Phys. Chem.*, 1994, **98**, 585-593.
62. C. Xu and B. E. Koel, *Surf. Sci.*, 1994, **304**, 249-266.
63. L. Nie, P. M. de Souza, F. B. Noronha, W. An, T. Sooknoi and D. E. Resasco, *J. Mol. Catal. A* 2014, **388-389**, 47-55.
64. W. Gao, W. T. Zheng and Q. Jiang, *J. Chem. Phys.*, 2008, **129**, 164705.
65. A. J. R. Hensley, Y. Wang and J.-S. McEwen, *Surf. Sci.* , 2014, **630**, 244–253.
66. M. L. Honkela, J. Bjork and M. Persson, *Phys. Chem. Chem. Phys.*, 2012, **14**, 5849-5854.
67. H. Orita and N. Itoh, *Appl. Catal. A*, 2004, **258**, 17-23.
68. L. Delle Site, A. Alavi and C. Abrams, *Phys. Rev. B*, 2003, **67**, 193406.
69. A. Javier, Y.-G. Kim and J. H. Baricuatro, *Electrocatal.*, 2012, **3**, 353-359.
70. J. E. Soto, Y.-G. Kim and M. P. Soriaga, *Electrochem. Commun.*, 1999, **1**, 135-138.
71. H. Ihm and J. M. White, *J. Phys. Chem. B*, 2000, **104**, 6202-6211.
72. N. H. H. Abu Bakar, M. M. Bettahar, M. Abu Bakar, S. Monteverdi, J. Ismail and M. Alnot, *J. Catal.*, 2009, **265**, 63-71.